PCCP

PAPER

# Combined excitatory and inhibitory coupling in a 1-D array of Belousov–Zhabotinsky droplets

Cite this: *Phys. Chem. Chem. Phys.*, 2014, **16**, 10965

Ning Li,†[a] Jorge Delgado,†[bc] Hector O. González-Ochoa,[ad] Irving R. Epstein[b] and Seth Fraden*[a]

Received 5th March 2014,
Accepted 16th April 2014

DOI: 10.1039/c4cp00957f

www.rsc.org/pccp

We study the dynamical behavior of one-dimensional arrays of ~100 μm diameter aqueous droplets containing the oscillatory Belousov–Zhabotinsky (BZ) reaction, separated by narrow gaps of a fluorinated oil. In this closed system, the malonic acid concentration decreases as the reaction proceeds. Starting with a low initial malonic acid concentration, we observe a series of attractors as a function of time in the following order: anti-phase attractors; in-phase attractors, which evolve into traveling waves; and mixed modes that contain either regions of in-phase droplets separated by anti-phase oscillators, or in-phase oscillators combined with non-oscillatory droplets. Most of the observations are consistent with numerical chemical models of the BZ reaction in which components that participate in the excitatory (bromine dioxide and bromous acid) and inhibitory (bromine) pathways diffuse between the droplets. The models are used to quantitatively assess the inter-drop coupling strength as a function of drop separation, drop size and malonic acid concentration. To experimentally establish the mechanism of excitatory coupling between the BZ droplets, we verify the transport through the fluorinated oil of chlorine dioxide and several weak acids, including malonic acid.

## 1. Introduction

Recent studies[1–8] of chemically coupled microdroplets containing the Belousov–Zhabotinsky (BZ) oscillating chemical reaction demonstrate that such emulsion systems are interesting experimental models for understanding coupled nonlinear chemical oscillators. These systems show collective behavior belonging to the same class of phenomena exhibited by numerous biological systems, ranging from single cell organisms to neuronal circuits. Specifically, the system studied here consists of drops of BZ solution of ~100 μm diameter immersed in oil. The approximately one nanoliter drops are stabilized by a surfactant and enclosed in a cylindrical capillary of inner diameter of 100 μm, forming a linear one-dimensional (1-D) array of about one hundred BZ drops, as illustrated in Fig. 1. The BZ reactants, intermediates and products partition into the oil phase to different degrees and can diffuse between the drops, causing the coupling. In contrast to previous work,[1,3,5,8] in which we studied drops in 1-D and 2-D geometries and observed a rich variety of dynamical attractor states ranging from all the drops oscillating with fixed phase shifts between neighboring drops, to stationary Turing states, as well as mixed states in which some drops were stationary and others oscillated, in this paper we study 1-D drop dynamics at extremes of high and low malonic acid concentration ([MA]). A previous paper[2] is devoted to theoretical modeling of the observations presented here. In the limit of low [MA], we also observe in-phase oscillations and traveling waves. All our models[2] suggest that the in-phase behavior at low [MA] is due to inter-drop coupling *via* excitatory species. Additionally, we observe mixed mode patterns in which some drops oscillate and others do not, as well as "local in-phase" behavior, in which pairs or small clusters of neighboring droplets are in phase with each other, but are out-of-phase with neighboring clusters. This behavior is consistent with multistable attractors resulting from a combination of inhibitory and excitatory coupling.[2] In the high [MA] limit, we also observe in-phase oscillations and traveling waves. However, our models[2] do not predict in-phase behavior at high [MA], indicating that our chemical mechanism of inter-drop coupling is incomplete.

In all cases we compare experiments on closed systems with theory for open systems in which the concentrations of malonic acid, sulfuric acid and bromate ion are assumed to remain constant. This enables us to identify stable attractors and to avoid modeling the poorly understood details of malonic acid consumption. As long as the fractional change in the concentrations of these

[a] *Department of Physics, Brandeis University, Waltham, MA 02454-9110, USA. E-mail: fraden@brandeis.edu*
[b] *Department of Chemistry, Brandeis University, Waltham, MA 02454-9110, USA*
[c] *División de Ciencias e Ingenierías, Universidad de Guanajuato, León, 37150, México*
[d] *División de Matemáticas Aplicadas, Instituto Potosino de Investigación Científica y Tecnológica (IPICyT), Camino a la Presa San José 2055, San Luis Potosí, 78216, México*
† Contributed equally.

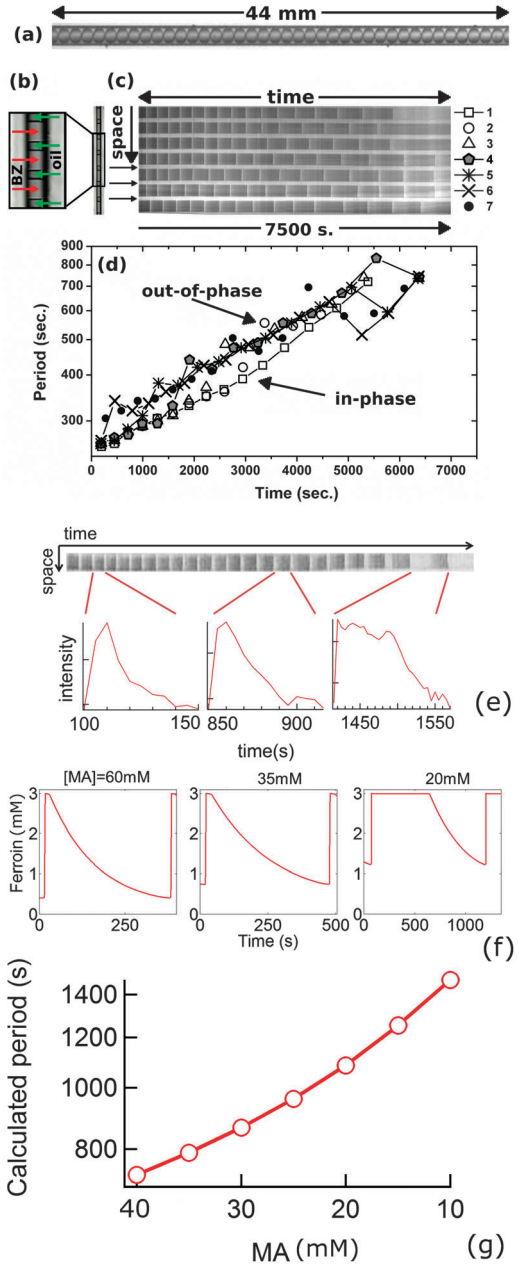


Fig. 1 BZ oscillations in a 1-D closed array of drops. (a) Photograph of section of a hydrophobized cylindrical capillary of 100 μm inner diameter filled with drops containing the Belousov–Zhabotinsky reaction. The drops are separated by fluorinated oil. (b) Magnified section of an unhydrophobized capillary containing BZ drops (red arrows) separated by oil (green arrows). Droplet diameter, $a$ = 120 μm. Oil gap, $b$ = 40 μm. (c) Space-time plot of seven drops shown in Fig. 1b. Three arrows indicate the oil gaps between drops, which appear as bright lines running parallel to the time axis, because the light transmitted through the oil gap is constant in time. Bright lines parallel to the space axis correspond to the oxidized state of the BZ reaction. (d) Period *vs.* time for the seven drops shown in the space-time plot of Fig. 1c. Initially, [MA] = 40 mM. (e) Transmitted light intensity through drop 6 (from left) from Fig. 10a as a function of time. The intensity profile as a function of time for the 2nd, 15th, and 22nd oscillations. (f) Calculated ferroin concentration *vs.* time for different concentrations of malonic acid, with $[BrO_3^-]$ = 600 mM and $[H_2SO_4]$ = 80 mM, $a$ = $b$ = 150 μm. (g) Calculated oscillation period *vs.* malonic acid concentration for a single BZ droplet, using default chemical conditions: $[BrO_3^-]$ = 300 mM and $[H_2SO_4]$ = 80 mM.

three chemicals is small, the experiments on the closed systems and our simulations of the open systems agree well. Here we consider systems in which the concentration of MA is smaller than the sulfuric acid and bromate ion concentrations, so the consumption of MA represents the greatest difference between the open and closed systems. To compare theory and experiment, we prepare a series of BZ emulsions as a function of [MA] and compare the initial behavior of each of these emulsions, which are closed systems, with the corresponding theoretical open systems. Pursuing the same logic, we reason that the time dependence of a single closed system can be qualitatively mapped onto a series of open systems with decreasing [MA].

Theoretical models of coupled BZ oscillators are necessarily simplified, not only because of the complexity of the chemical kinetics of the reaction,[9] but also because the degree to which the chemicals partition into the oil and their reactivity within the oil are poorly known. However, because the kinetics within the microdroplets are the same as in the macroscopic BZ reaction, one can make use of well-established detailed models[10] as a starting point.[3,5]

We model the coupled BZ drops at three levels of approximation. The most realistic consists of a finite element model (COMSOL®) of the reaction-diffusion equation in 1-D, 2-D and 3-D, where each drop is modeled as a point, disk or sphere, respectively. Only minor differences are observed between 1-D, 2-D and 3-D drops arranged periodically in a straight line. The capillary walls are treated as a no-flux boundary condition. The reaction term is modeled using the 7-variable FKN model as detailed in previous work.[1] Chemicals are allowed to diffuse within the drop and the oil and to exchange between the two phases governed by a partition coefficient, $P$, defined as the ratio of equilibrated concentrations of a particular species in the oil and water phases ($P = c_{oil}/c_{water}$). These boundary conditions at the oil/water interface are enforced in COMSOL using the "stiff" method[11] to have to right partition coefficients. Each chemical species has the same diffusion constant in the oil and the water. No chemical reactions are allowed to occur in the oil, which we find experimentally is not the case. However, we argue that this simplification is justified for most of the cases studied here. Models of intermediate complexity approximate each spatially extended drop as a 7-variable FKN oscillator confined to a single point. The BZ drops are diffusively coupled to their nearest neighbors. This class of models, consisting of a ring of diffusively coupled point-like chemical reactors, was first introduced by Turing.[12] We numerically solve the model using Matlab® as described in an earlier computational study.[1] The diffusion across a 100 μm sized droplet takes very little time compared to the oscillation period, so the droplets are oscillating homogeneously. Thus the point model is justified. The point model and finite-element model give similar results for 1-D systems. Finally, at the most abstract level, we construct a single variable phase oscillator model,[13] in which the phase coupling function is derived from the point oscillator model.

In our numerical investigations of open systems, steady state dynamical patterns are identified as attractors. Technically, no attractors exist in the closed system, because the only steady

state is equilibrium. However, as we previously demonstrated, our closed system gives rise to ''pseudo-attractors'' that maintain an oscillatory pattern for many periods and have the same dynamic behavior as the true attractors found in simulations of the corresponding open system.[1]

We also experimentally explore the source of stability of the in-phase attractors in our system; experiments to measure the transport of several BZ-related species through our fluorinated oil suggest that excitatory coupling takes place *via* exchange of bromine dioxide radical ($BrO_2^{\bullet}$) and bromous acid ($HBrO_2$) among droplets, while the inhibitory coupling is conveyed by bromine ($Br_2$).

## 2. Experimental

Arrays of water droplets in oil are generated using flow focusing microfluidic technology as described in our previous work:[1] A microfluidic chip fabricated from polydimethylsiloxane (PDMS) allows the injection of equal amounts of different aqueous streams into a central mixing channel. This channel ends in a nozzle of 50 μm diameter, where streams of fluorinated oil coming perpendicularly from both sides produce droplets by flow focusing. After the nozzle, the channel widens to 100 μm diameter with a square cross section. Drops of this volume oscillate at most a few times if stored in a PDMS channel. Previously we argued this is due to permeation of bromine into the PDMS. If the ratio of the volume of the PDMS chip to the volume of the BZ solution is large, then the oscillating reaction ceases.[3] Therefore we export the drops from the PDMS chip to a hydrophobized glass capillary. In standard soft lithography microfluidics,[14] three of the four walls of the microfluidic channel are made from PDMS, which is then sealed to a glass slide to form the fourth wall. Instead, we use a 5 mm flat slab of PDMS to seal the channel and cut the assembled device perpendicular to the channel. Having four soft walls allows us to insert a cylindrical hydrophobized capillary of 100 μm inner diameter (170 μm outer diameter) directly into the 100 μm channel emerging from the cut side of the microfluidic chip. Unless otherwise specified, all experiments described here are conducted in capillaries of this size.

Previous to experiments, capillaries are hydrophobized using a vacuum chamber in which capillaries and a small amount of liquid (tridecafluoro-1,1,2,2-tetrahydrooctyl)trichlorosilane are placed. We reduce the pressure in order to evaporate the silane, which enters the capillaries *via* gaseous diffusion. The trichlorosilane group of this molecule reacts with the oxygen groups of the silica on the glass surface, covering it with fluorocarbon tails.[15] After two hours in the vacuum chamber, which is sufficient for hydrophobizing the capillaries, we remove the capillaries. Air stops the reaction, because oxygen reacts with the chlorosilane groups. The oil used in this work is a perfluorinated oil, HFE 7500: 3-ethoxy-1,1,1,2,3,4,4,5,5,6,6,6-dodecafluoro-2-trifluoromethyl-hexane (3M Corp., St. Paul, MN, USA, dielectric constant = 5.8). Since this is the only oil used, we refer it as ''the oil''. An amphiphilic PEG-PFPE fluorinated block copolymer dissolved at a concentration of 2% by volume in the oil serves as a surfactant for aiding droplet formation and preventing droplet coalescence. The surfactant was provided by RainDance Technologies, Lexington, MA, USA and is similar to a surfactant[16] described in the literature. A commercial version of this surfactant is now available (RAN Biotechnologies).

To form BZ droplets in oil using this chip, we inject malonic acid (Sigma-Aldrich) and sulfuric acid (Fisher) at twice the final desired concentrations in the droplet in one aqueous stream. The second aqueous stream contains sodium bromate (Fisher), ferroin indicator (Aqua Solutions) and $Ru(bipy)_3^{2+}$ (Sigma-Aldrich) also at twice the final desired concentrations. Unless otherwise noted, $[BrO_3^-]$ = 300 mM, $[H_2SO_4]$ = 80 mM, [ferroin] = 3 mM and $[Ru(bipy)_3^{2+}]$ = 0.4 mM in the droplets in all our experiments. We use ferroin as a BZ catalyst and $Ru(bipy)_3^{2+}$ as a co-catalyst and photosensitizer. The ferroin contained in the BZ drops also serves as a dye indicator, changing from blue (oxidized ferroin) to red (reduced ferriin) depending on its oxidation state. Capillaries with identical BZ droplets equidistantly spaced by identical volumes of oil are sealed using 5 minute epoxy, attached to a microscope slide and observed with a CCD camera through a microscope. If the capillary is inadequately sealed, gas bubbles evolve, causing the drops to move, which disturbs the chemical dynamics and disqualifies the experiment.

The capillary is illuminated in transmission with a 510 ± 10 nm notch interference filter inserted into the light path to maximize the transmission of light when the BZ drops are in the oxidized state. Visually, the BZ drops appear bright in the ferroin oxidized state (ferriin) and dark in the reduced state. The light intensity transmitted through the transparent oil separating the drops is constantly bright during the entire experiment because ferroin does not diffuse out of the drops into the oil. Our field of vision, in which up to 20 droplets can be observed, is located at the center of the sealed capillary. There are at least 15 additional droplets to each side of this central region. In most cases the drops have a few percent variation in size and spacing. However, we did not quantitatively investigate the effects of variable drop size and spacing on the dynamics, which will be the subject of future work. We construct space-time plots by acquiring the space data at a fixed time from a single image by extracting the intensity of transmitted light from a single row of pixels along the capillary axis. The time data is acquired by repeating this process from a set of digital images taken at constant (3–5 s) intervals over the course of an experiment. In some experiments, the droplets are initially synchronized in-phase using the photosensitivity of the $Ru(bipy)_3^{2+}$ co-catalyst to suppress oscillations by illuminating the capillary with intense 450 nm light for about 10 min.[5] The diameter of the droplets is defined as their width along the capillary in the axial direction. The distance between droplets is taken as the length of the gap between the boundaries of adjacent droplets measured along the axis of the capillary.

Droplets of chlorine dioxide, $ClO_2^{\bullet}$, in water are generated using the PDMS microfluidic chip. In one aqueous stream, we introduce sodium chlorite at 0.5 M ($NaClO_2$, Acros Organics, 80% pure), pH = 6, and in the other aqueous stream we place nitric acid in excess: 4.0 M (Fisher). The acidification of $NaClO_2$

produces $HClO_2$, which undergoes a disproportionation reaction and forms $ClO_2^{\bullet}$.[17] For the conditions used in the droplets, spectrophotometric measurements in bulk reveal a maximum concentration of $ClO_2^{\bullet}$ of about one tenth of the initial chlorite concentration approximately 20 min after the mixing of the reactants. From this observation, we can estimate the maximum concentration of $ClO_2^{\bullet}$ in the droplets as $\sim$50 mM. To observe the concentration of $ClO_2^{\bullet}$ in the microfluidic drops, we place a 400 nm interference notch filter in the microscope illumination path. Although both $ClO_2^{\bullet}$ and $HClO_2$ absorb at this wavelength, the molar extinction coefficient of $ClO_2^{\bullet}$ is at least one order of magnitude greater than that of $HClO_2$.[18]

For experiments on the transport of weak acids, thymol blue, iodoacetic acid and chloroacetic acid were obtained from Sigma-Aldrich, Acros Organics and Fisher, respectively.

# 3. Results and discussion

This work consists of four sections. (1) The quantitative relationship between our experiments on a closed BZ system and the theory of an open system. (2) The origin of inhibitory coupling between neighboring BZ droplets and the measurement of the coupling strength. (3) A phase model for weakly coupled BZ oscillators. (4) The chemical mechanisms of excitatory coupling, which gives various in-phase behaviors. These points will be discussed in the following subsections.

## 3.1 Consumption of malonic acid in closed system

In Fig. 1 we present an experiment that is representative of many of the phenomena observed for BZ drops at low malonic acid. Consider the complex behavior illustrated in the space-time plot of Fig. 1c. In the beginning, drops are synchronized to begin oscillating in-phase, but with time drift out-of-phase. At the end, some drops (*e.g.*, #4, #5 and #6) switch back to in-phase, while some others (*e.g.*, #2) stop oscillating. The oscillation period is longer for drops that are out-of-phase with their neighbors than for in-phase drops. The period increases with time, and the oscillation waveform of the oxidation/reduction of ferroin changes with time. All of these phenomena will be explained as a consequence of the consumption of malonic acid, leading to increased inter-drop coupling.

Proceeding in detail, Fig. 1a is a photograph of a 100 μm inner diameter hydrophobized capillary filled with BZ drops that are in contact with each other. The oil wets the capillary, and surface tension causes the drops to adopt a cylindrical shape with hemispheres on the end. Fig. 1b shows 120 μm long BZ drops (red arrows) separated by 40 micron oil gaps (green arrows) in a non-hydrophobized capillary. Fig. 1c shows a space-time plot of the BZ drops in Fig. 1b with initial [MA] = 40 mM. With these initial conditions, the drops spontaneously oscillate. All the drops are initially synchronized to have the same phase by first suppressing the oscillations *via* strong illumination for several minutes and then removing the light from all the drops simultaneously. During the first two oscillations, drops #1 through #6 oscillate in-phase while drop #7 is out of phase. With time, the remaining drops sequentially fall out of phase starting with drop #6, then #5, *etc*. By the 12th oscillation, all seven drops are out of phase with each other. However, at the 14th oscillation, drops #5 and #6 synchronize in-phase and at the 15th oscillation, drops #4, #5, and #6 are synchronized in-phase. At this time, drops #1, #2, and #3 stop oscillating altogether. During the out-of-phase regime of the first 15 oscillations, the phase-shift between adjacent droplets is never $\pi$ (180°). For instance, the phase-shift between droplets #6 and #7 is less than $0.7\pi$ during most of the experiment. As previously reported, such a condition during the out-of-phase regime can be considered as a mark of weak inhibitory coupling.[1] Our explanation for the evolution over time from in-phase to out-of-phase behavior for the first 15 oscillations is that the initial in-phase condition, set by the imposition of light, is unstable, and the system evolves towards the stable anti-phase attractor. However, over time [MA] decreases as it is consumed in the closed system. Our numerical studies of a pair of interacting drops in an open system reveal that at low [MA] the diffusive coupling of $Br_2$, $HBrO_2$, and $BrO_2^{\bullet}$ leads to bistability between in-phase and out-of-phase attractors, which explains why after 15 oscillations some of the drops adopt an in-phase attractor.[2] Finally, at lower [MA] some drops stop oscillating. We identify those drops with stationary Turing states, triggered by strong inhibitory coupling, which are predicted to be bistable with in-phase attractors at very low [MA].[2]

Fig. 1d shows the period as a function of time for each of the seven droplets as numbered on the space-time plot. The periods for the droplets that oscillate in-phase and for the droplets oscillating out-of-phase with adjacent neighbors evolve along two different lines. At the beginning of the experiment, only one droplet (#7) is out of phase with the other drops and lies on the out-of-phase line, which has a longer period than the in-phase drops at the corresponding time. Once a droplet moves from the initially unstable in-phase behavior to the more stable out-of-phase attractor, the period increases and the drop switches to the upper line. This process occurs more gradually in droplet #1, which does not go back to in-phase interaction. At a later stage some droplets, *e.g.* #5 and #6, return to their earlier in-phase behavior and consequently, their period decreases. Fig. 1e shows the temporal behavior of a single drop that is extracted from an array of interacting drops (see Fig. 10a) with initial conditions [MA] = 60 mM, $[BrO_3^-]$ = 600 mM and $[H_2SO_4]$ = 160 mM. The intensity of transmitted light, which is proportional to the ferroin concentration, is also plotted as a function of time. There is a noticeable lengthening of the period and change of duty cycle, defined as the fraction of each cycle spent in the oxidized state, with time. Oscillations with a long duty cycle of the oxidation state are observed in low [MA] solutions, while the oscillations have a short duty cycle at high [MA].[2,19] Fig. 1f shows how the ferroin concentration, calculated in the point oscillator model for a pair of coupled drops in steady state, varies as a function of time for different values of [MA]. Matching the waveform from the calculation with the observed waveforms in Fig. 1e allows us to estimate how [MA] varies as a function of time. For this range of conditions we find $[MA](t\,[s]) \approx 60\ mM - 0.03\ [mM\ s^{-1}]\ t\ [s]$. Fig. 1g shows the numerically calculated

 

period (based on the FKN model) of a single BZ droplet as a function of malonic acid concentration. The period increases as [MA] decreases; thus all the observations in Fig. 1 are consistent with a decreasing concentration of malonic acid in the drops with time.

### 3.2 Modeling inhibitory coupling strength: finite element analysis

Previous experimental studies[1,3,5] of a large number of equally spaced droplets inside a cylindrical capillary found anti-phase attractors, in which adjacent drops oscillated 180° out of phase with each other. This occurred for a wide range of droplet diameters ($a$), length of oil gap between droplets ($b$) and intermediate [MA]. This anti-phase behavior was explained to be a result of inhibitory coupling of the drops, which arises from the diffusion of bromine ($Br_2$) between droplets. For clarification, in the aqueous BZ reaction, inhibition is carried out by bromide ($Br^-$), but this charged species does not partition into the oil. However, $Br_2$, which is nonpolar, partitions readily into the oil and diffuses from drop to drop. Once inside the aqueous phase, $Br_2$ brominates MA, generating $Br^-$; thus $Br_2$ acts as the carrier of inhibition, and not as the inhibitor itself: $Br_2 + MA \rightarrow BrMA + Br^- + H^+$. Our results suggest that this bromination can be characterized by an effective rate constant $k_{eff} = 10\ [s^{-1}] + 29\ [M^{-1}\ s^{-1}]\ [MA]$.

**(a) Origin of coupling: diffusive flux.** In Fig. 2a, we present the results of solving a reaction-diffusion finite element model of the FKN equations. The model accounts for the permeation of the activators bromine dioxide and bromous acid, as well as bromine, which couples to the inhibitory reaction, into the oil separating the BZ drops. We modeled the drops as spheres contained in a cylindrical capillary whose inner diameter matches the sphere diameter. We also modeled the spheres as lines in 1-D and disks in 2-D and found only minor quantitative differences between the 1-D, 2-D and 3-D solutions. To investigate how two drops interact, we ran simulations on three configurations: two drops of diameter $D$ separated by $0.1D$ to represent conditions of strong coupling, two drops of diameter $D$ separated by $10D$ to represent conditions of weak coupling, and a single drop as a reference for comparison. In Fig. 2 the drops are 200 μm in diameter filled with BZ solution with [MA] = 20 mM in a 2-D, rectangular, impermeable container filled with oil.

The observation that the period of a pair of 180° out-of-phase droplets is longer than that of a pair of drops with 0° phase shift,[3] which was described in Fig. 1d, can be explained by examining Fig. 2b, in which the concentration of $Br_2$ in the center of the left drop and in the oil gap separating the two drops is plotted as a function of time. Bromide ($Br^-$) inhibits the BZ oscillation. Injection of a pulse of $Br^-$ into a homogeneous stirred BZ solution lengthens the period of oscillation, because additional time is required for removing it, which is required in order to start the autocatalytic BZ step.[20,21] However, it is $Br_2$ and not $Br^-$ that is transmitted between drops. $Br_2$ is rapidly produced in a drop when it undergoes the oxidation transition. If two drops are out-of-phase, then the pulse of $Br_2$ produced in one drop (the transmitter) diffuses to its neighbor (the receiver), where it is converted to $Br^-$, thereby delaying the oscillation of the receiving drop.

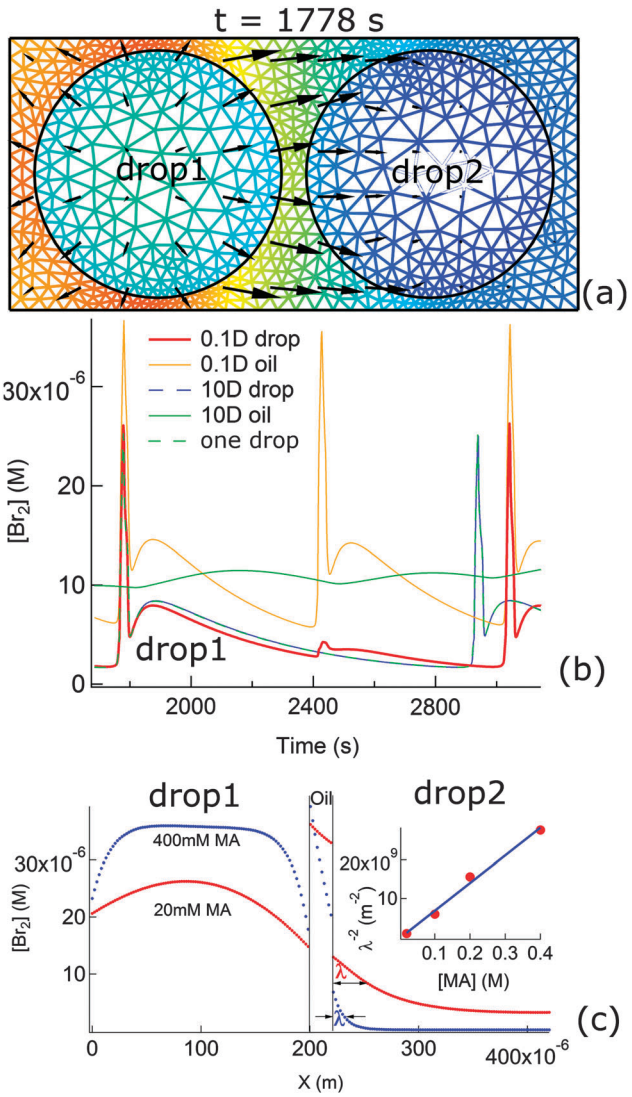


Fig. 2 Bromine coupling. (a) Mesh used in a finite element calculation in 2-D of two 200 μm drops of BZ fluid immersed in oil. The full FKN model was solved on each vertex with the following conditions: [MA] = 20 mM, 20 μm oil gap. The boundary condition at the oil/BZ interface was set by the partition coefficient, $P_{Br_2} = [Br_2]_{oil}/[Br_2]_{BZ} = 2.5$, $P_{BrO_2} = [BrO_2]_{oil}/[BrO_2]_{BZ} = 3$, $P_{HBrO_2} = [HBrO_2]_{oil}/[HBrO_2]_{BZ} = 0$. Here the partition coefficient for $BrO_2$ was set to an unphysical value 3 to test the effect of excitatory coupling in simulation. The same coupling strength can be obtained by lowering this value to 1 and using $P_{HBrO_2} \approx 0.01$. A no-flux boundary condition was set at the exterior boundary. The time corresponds to 1778 s in Fig. 2b. Arrows show flux of $Br_2$ and color shows $[Br_2]$, with orange high and blue low. (b) $[Br_2]$ as a function of time in the oil between the drops at the midpoint on the symmetry axis and in the center of the leftmost drop. Two separations of drops are calculated; 2000 μm ($10D$; 10 times drop diameter) and 20 μm ($0.1D$; 0.1 of drop diameter). A single drop (one drop) in the larger geometry is also calculated. (c) $[Br_2]$ as a function of distance across the simulation box of Fig. 2a for two different [MA]. Concentrations are plotted at 1778 s, just after the left drop undergoes an oxidation transition. The range ($\lambda$) that the $[Br_2]$ penetrates into the neighboring drop is a measure of the coupling strength. $\lambda$ is defined as the distance it takes for $[Br_2]$ to drop halfway to its minimum. Decreasing [MA] increases $\lambda$ as shown in the inset.

The dashed blue curve ("$10D$ drop") in Fig. 2b shows the temporal variation of $[Br_2]$ in the center of drop 1 in a closed

container with drop 2 located 10 diameters away. In a second calculation involving a container with a single drop, the temporal variation of $[Br_2]$ is shown as the dashed green curve ("one drop"). The location of drop 1 and the size of the container were the same as in the "10*D* drop" calculation, but drop 2 was removed and replaced with oil. The temporal variation of $[Br_2]$ for two drops separated by 10 diameters ("10*D* drop") is indistinguishable from the case of one drop in a sealed container of the same size ("one drop"), which indicates that when drops are 10 diameters apart they are decoupled.

When the drops are brought close to each other (a gap of 0.1 drop diameter) the $Br_2$ concentrations are significantly distorted, as shown in Fig. 2b "0.1*D* drop". Compared to the case of drops far apart, during half the cycle the level of $Br_2$ inside drop 1 is depressed and in the other half of the cycle the $Br_2$ level in the same drop is elevated. The explanation is that as the drops are out of phase with each other, when drop 1 undergoes the oxidation transition at $t = 1778$ s, it emits a large amount of $Br_2$ at the moment when the $Br_2$ level in its neighbor, drop 2, is low. Thus drop 2 acts as a sink of $Br_2$ leading to a reduction in $[Br_2]$ in drop 1 compared to the case when the drops are greatly separated. Likewise, when drop 2 oxidizes at $t = 2400$ s, it emits a pulse of $Br_2$, raising the $Br_2$ level of drop 1 above its value when the drops are far apart and causing the period of oscillation to lengthen. Note that the diffusive coupling is fast when the drops are separated by an oil gap of 20 μm; thus drop 1 receives the pulse of $Br_2$ less than 1 s after it is emitted by drop 2 at 2400 s.

Fig. 2a shows the flux and concentration of $Br_2$ and Fig. 2b plots the concentration as a function of time. We also measured the total flux in and out of a drop as a function of partition coefficient in steady state conditions (not shown). Under these conditions the total flux is zero. We found that the flux out of a drop increased monotonically with partition coefficient in steady state, however it is not clear how to quantitatively relate the chemical flux to the degree of dynamical coupling between drops.

**(b) Dimensional analysis and *S* parameter.** One heuristic measure of the coupling strength is the dimensionless number $S = (P_{Br_2}D)/(a(a + b)k_{eff}) = \mu/k_{eff}$, which is the ratio of two rates: $\mu = (P_{Br_2}D)/(a(a + b))$, the rate of diffusive transport between BZ drops of the inhibitor bromine separated by an oil gap, and $k_{eff}$, the effective rate constant characterizing the consumption of $Br_2$, which as described previously, occurs *via* bromination of malonic acid. Here $P_{Br_2}$ is the partition coefficient, $D$ is the diffusion coefficient of bromine, $a$ is the BZ droplet size, $b$ is the oil gap size. The derivation of $\mu$ (assuming the drop–oil interface is flat) is presented elsewhere;[1] an alternative expression for $\mu$ using the Derjaguin approximation considering the actual curvature of the drops is derived in another work.[8]

In order to estimate $k_{eff}$, we plot the concentration of $Br_2$ as a function of distance in Fig. 2c at $t = 1778$ s, just after the drop on the left is oxidized, as depicted in Fig. 2a. If the time for bromine to diffuse across a drop is short compared to the oscillation period, then $\partial c(x,t)/\partial t$ can be neglected. For $D = 10^{-5}$ [$cm^2$ $s^{-1}$] and $a = 10^{-2}$ [cm] the time for $Br_2$ to diffuse across the drop, $\tau_D = 10$ s, is much shorter than the oscillation period, which is greater than 300 s. The solution to the time-independent reaction-diffusion equation is an exponential with a characteristic decay length $\lambda = \sqrt{D/k_{eff}}$. We define $\lambda$ as the distance from the water/oil interface to the point that the $Br_2$ concentration is reduced halfway to its minimum. We find $\lambda$ is constant in time, supporting the contention that $\partial c(x,t)/\partial t$ is negligible. In Fig. 2c we plot $\lambda^{-2}$ *vs.* malonic acid concentration and numerically find that $k_{eff}$ is linear in malonic acid concentration; $k_{eff} = (70\ M^{-1}\ s^{-1})$ ([MA]). This result is roughly consistent with the 7-variable mechanism, which suggests that $k_{eff}$ should be equal to $k_6 + k_7 = (10 + 29\ [MA]\ (M^{-1}))\ s^{-1}$.

Two factors, one chemical and one geometrical, control how strongly the bromine emitted from one drop influences the oscillation of the receiving drop. In the limit of $S = (PD/a(a + b))/k_{eff} \ll 1$, the drops are weakly coupled. Chemically, $S$ decreases when $k_{eff}$ is increased. This is accomplished by increasing (MA), which increases $Br_2$ consumption inside a drop, leaving less $Br_2$ to diffuse between drops. Furthermore, at high [MA], the $Br_2$ that is emitted from one drop and transported through the oil is rapidly consumed in the receiving drop upon arrival and therefore only slightly increases the $Br_2$ concentration in the receiving drop. Geometrically, increasing the separation of the drops weakens coupling. As transport is diffusive, this both increases the transport time and broadens the transmitted pulse, thereby reducing the diffusive transport between drops. In the limit of $S \gg 1$ the drops are strongly coupled. Decreasing (MA) strengthens coupling because the reaction rate $k_{eff}$ decreases. When $k_{eff}$ is small and $S$ is large, bromine diffuses from the emitting drop to the receiving drop faster than the receiving drop can consume the transmitted bromine. Consequently, the concentration of bromine in the receiving drop will be significantly increased, resulting in either a phase shift in the limit cycle, or, for very strong coupling, distorting the shape of the limit cycle. Alternatively, the coupling strength can be increased by decreasing the drop separation, which increases the inter-drop diffusive transport. We previously observed that as either (MA) or drop size decreases, more drops stop oscillating out of phase and enter a non-oscillatory Turing state, in which drops are maintained far from equilibrium in either the reduced or oxidized state.[1] This observation is consistent with theoretical work on coupled BZ oscillators, which predicts that a stationary Turing state is reached as the inhibitory coupling is increased.[5,22]

### 3.3 Phase model for weakly coupled oscillators

We now consider a second measure of the coupling strength. Drops that beat in synchrony are coupled. Experimentally and numerically we have found that for a pair of drops there are three limiting synchronous behaviors: in-phase, in which the oscillators have the same phase, anti-phase, in which the oscillators beat 180° out of phase[13] and multistable, in which multiple attractors are possible, depending on initial conditions. A natural measure of the strength of the coupling is the degree to which one drop affects the phase of its neighbor, characterized by the phase coupling function,[23–25] $H$. The phase model is

$$\dot{\theta}_1 = \omega_0 + H(\theta_2 - \theta_1) \quad (1a)$$

$$\dot{\theta}_2 = \omega_0 + H(\theta_1 - \theta_2) \quad (1b)$$

 

with $\theta_i$ the phase of the oscillator, $\omega_0$ the frequency of each oscillator when uncoupled, and $H$ the phase coupling function. If $H$ does not change sign, then there is only one attractor, either in-phase or anti-phase, set by the sign of the derivative of $H$. The number of zero crossings of $H$ sets the number of multistable attractors (see Kuramoto,[13] eqn (5.2.18)).

**(a) Single species effect on coupling.** Before we calculate the phase coupling function, we first numerically explore the qualitative effect transmitted chemicals have on the synchronization of coupled drops. We do this by allowing only one species at a time to diffuse between drops and numerically solve our point oscillator and finite element models. The naïve expectation is that coupling through inhibitory species would lead to out-of-phase synchronization and excitatory coupling leads to in-phase synchrony. If a pair of oscillators are inhibitory coupled, then each delays the other, and their phase difference will grow to the largest possible value, 180°. Such a coupling is called "phase repulsive".[13] By the same logic, coupling of excitatory species would lead to in-phase coupling, because each oscillator stimulates the other, shortening their phase difference, referred to as "phase attractive" coupling.[13]

We consider, one at a time, transport of the inhibitory species, $Br_2$ and $Br^-$, and the excitatory species, $HBrO_2$ and $BrO_2^\bullet$, in the point oscillator and finite element models. In the point oscillator model, if we allow only $Br_2$ to transport between drops and limit the partition coefficient $P_{Br_2} < 400$, the drops synchronize out-of-phase. While the measured value is $P_{Br_2} = 2.5$, for the sake of completeness we consider $P_{Br_2} > 400$, in which case a Turing/in-phase (depending on initial condition) mixed state is found. For the finite element model, the result is qualitatively the same, however the partition constant at which the behavior switches from out-of-phase to in-phase occurs at an 8-fold lower value, $P_{Br_2} = 50$, than in the point oscillator model. The ion $Br^-$ is charged and therefore not expected to partition into the oil. However, again for the sake of completeness, we consider how inter-drop transport of $Br^-$ influences synchronization. We find that in the point oscillator model, for a partition coefficient $P_{Br_2} < 0.1$, the drops synchronize out-of-phase. For larger partition coefficients the behavior first becomes bistable between out-of-phase and in-phase and then solely in-phase. The same qualitative behavior is observed for the finite element model. These two examples demonstrate that purely inhibitory coupling can lead to in-phase synchronization, contrary to our naïve expectation, but only when the partition coefficients are unphysically high. When in-phase synchrony occurs, the drops are resetting, by which we mean that the oxidation transition of one drop induces an immediate oxidation transition in its neighbor. We note that it is possible in principle for in-phase synchrony in coupled nonlinear oscillators to occur without resetting, but we never find this in our experiments or simulations. The intuitive description is that at high inhibitory coupling strength, two drops behave as one. With only excitatory coupling (restricting transport between drops to either of the two activators, $HBrO_2$ or $BrO_2^\bullet$), only in-phase synchronization is observed.

In other words, weak inhibitory coupling is phase repulsive and excitatory coupling is phase attractive. Strong coupling, whether inhibitory or excitatory, produces in-phase synchrony. The dynamical behavior of coupled drops is summarized in Fig. 3a. For pure $Br_2$ coupling, we identify the boundary between weak and strong coupling with the phase transition between out-of-phase and in-phase coupling. Using the values for the point oscillator model at the transition, $a = b = 150$ μm, [MA] = 200 mM, $P_{Br_2} = 400$ and $k_{eff} = 70$ [MA (M)] ($M^{-1}$ $s^{-1}$), the coupling strength $S = (PD)/(a(a + b)k_{eff}) = 0.63$; thus for this case the transition from weak to strong coupling occurs at $S \approx 0.6$.

**(b) Dynamical phase boundary and *S* contour.** To test further the conjecture that $S$ is a measure of coupling strength, we calculated the phase behavior using COMSOL for two drops that are coupled solely by the diffusion of bromine through the oil. The result is plotted as a function of [MA] and drop size for the case of oil gap equal to drop diameter and $P_{Br_2} = 2.5$, shown in Fig. 3b. Superimposed are green contour lines of constant coupling strength, $S$. If $S$ is a measure of coupling strength, then the boundary between the anti-phase (AP) oscillatory and stationary Turing states should occur for a constant value of $S$. Fig. 3b shows that the boundary corresponds roughly to $S \approx 0.1$, which supports the contention that the dimensionless parameter $S$, governs the dynamical behavior of the coupled BZ drops.

Additionally, for the case of bromine-only coupling, we calculated the dynamical phase boundary between anti-phase and stationary Turing states as a function of drop size $a$ and oil gap size $b$ using COMSOL and superimposed $S$ contours as shown in Fig. 3c. While the construction of the point model requires that the phase boundary is a function of $a \times (a + b)$, the functional form is not specified. In particular, there is no reason to suppose that the phase behavior scales as inversely proportional to $a \times (a + b)$, as is demonstrated in Fig. 3c. Furthermore, there is no such constraint on the phase boundary in the finite element models, as those equations do not have a unique form of non-dimensionalization. We interpret the results of Fig. 3c to mean that small drops are strongly coupled and that drop–drop coupling is relatively insensitive to drop separation. Experimental study of the dynamical behavior of drops as a function of size and separation will be the subject of future work.

**(c) Phase coupling function *H*.** Next we calculate $H$, the phase coupling function. Using the point oscillator model, we numerically calculate the phase coupling function (see eqn (5.2.17b) of Kuramoto,[13] or eqn (10.15) of Izhikevich[25]) for two identical coupled BZ drops as a function of drop diameter, drop separation, and [MA]. We consider that the following 3 components of the Turing point oscillator model have non-zero partition coefficients; $P_{Br_2} = 2.5$, $P_{BrO_2} = 1$, and $P_{HBrO_2} = 0.1$. The first two were estimated from experiment; the last was obtained by varying $P_{HBrO_2}$ until the best fit between experimental and calculated dynamical phase diagrams was obtained. Thus $P_{HBrO_2} = 0.1$ is a prediction of our point oscillator model. Using the finite element model we obtained $P_{HBrO_2} = 0.01$. While there were quantitative differences between the two models, their qualitative behavior was similar.

There are two ways to calculate $H$. One is indirectly, as done by Kuramoto,[13,24] using the phase response curve of a single drop, which in principle could be calculated from the point oscillator model. Instead we obtain $H$ directly by numerically

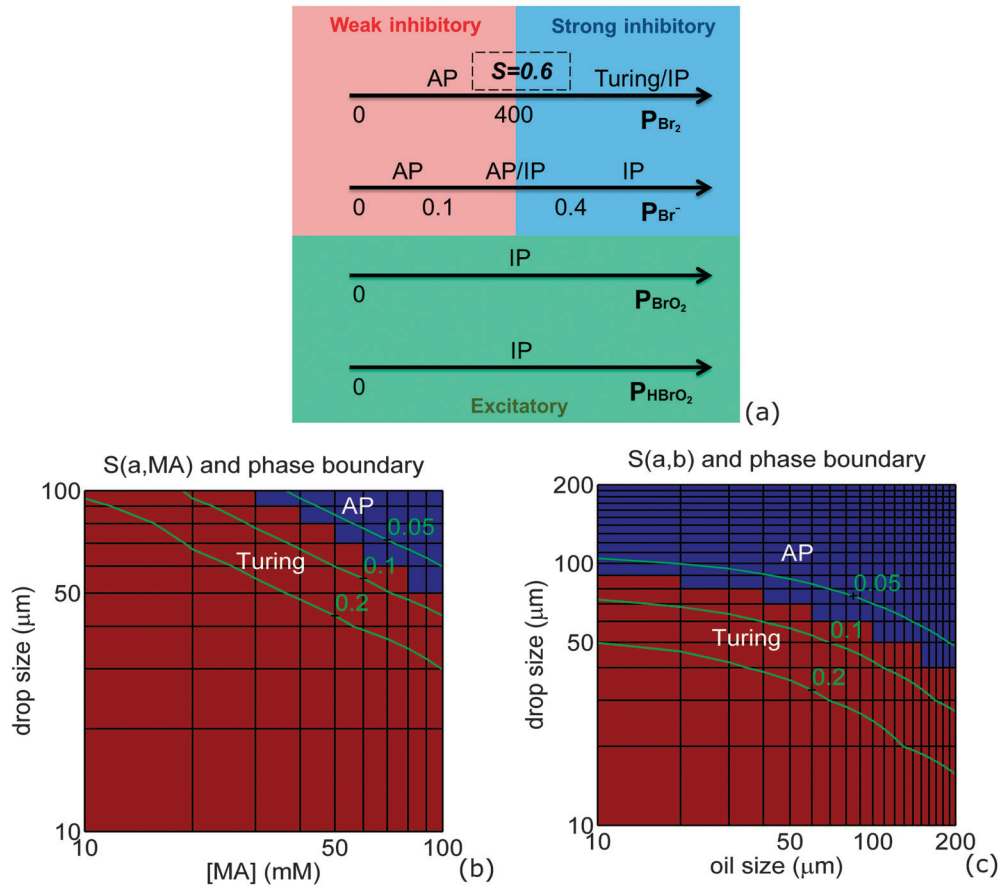


Fig. 3 Dynamical phase boundary and coupling strength $S$. (a) Calculated in the point-oscillator model with $a = b = 150$ μm, and [MA] = 200 mM. Only one chemical species at a time is allowed to diffuse between two drops. Four species are considered; two inhibitory and two excitatory. Phase behavior; AP; anti-phase oscillation. Turing (stationary); non-steady state. IP; in-phase oscillation. "AP/IP" indicates a multistable state. The results are qualitatively the same as those obtained from the finite element analysis (not shown). The partition coefficient at the phase transition is indicated for the point oscillator model. For $Br_2$ in the point oscillator model, the coupling strength $S = 0.6$ at the phase transition point. (b) Phase diagram as a function of drop size and malonic acid concentration (log scale) calculated using COMSOL (1-D) for two BZ drops coupled through only bromine with partition coefficient 2.5 and $a = b$. The dark red region is in a stationary Turing state, while the blue region is anti-phase oscillatory. Superimposed green lines are contour lines of coupling strength $S$; the numbers are the values of $S$. (c) Similar to Fig. 3b, phase diagram as a function of drop size and oil separation with [MA] = 60 mM.

calculating the phase shift that one drop imposes on its neighbor[26] after one period. Consider two point oscillators that are uncoupled ($H = 0$) and have a constant phase shift $\theta$. Since they are uncoupled $\dot{\theta}_i = \omega_0$. The ferroin concentration of these drops is plotted as a function of time in Fig. 4a (blue curves). At an arbitrary time, labeled $t = 0$ in Fig. 4a, we couple the two drops *via* the oil and plot the ferroin concentration for the coupled drops as a function of time (red curves). After one period of the uncoupled drop ($\tau$), the phase shift of drop 1 ($\Delta\theta$), relative to its phase when uncoupled is calculated and in Fig. 4b is plotted as a function of $\theta$ for four different values of malonic acid. $\Delta\theta/\tau$ is equal to the phase coupling function called $\Gamma$ by Kuramoto in eqn (5.2.17)[24] and $H$ by Izhikevich in eqn (10.16).[25] We use units of phase that vary between 0 and 1. The phase shift is unambiguous, because the coupled and uncoupled drops move on the same limit cycle, $x(t)$, where $x$ represents the 7 chemical variables in the FKN model. We numerically verified that $\Delta\theta$ is independent of the time when the two drops are coupled; for example, if the drops in Fig. 4a are coupled beginning at $t = 50$ s or $t = -50$ s, $\Delta\theta$ is the same as calculated for $t = 0$. In Fig. 4a, the time when $\Delta\theta$ is calculated is indicated as a dashed line. The value of $\Delta\theta$ is slightly less than $\Delta\theta'$, the phase difference between the expected oxidation transition for an uncoupled drop and for the same drop after it is coupled. However, $\Delta\theta'$ is notable because it is readily measurable.[26] As shown in Fig. 1, we measure the ferroin concentration during the entire cycle, from which it is possible in principle to extract $\Delta\theta'$. However, in practice, while numerically calculating $\Delta\theta$ is easy, experimentally it is subject to a large uncertainty. The sign of the phase shift tells whether or not the coupling is phase attractive (negative) or phase repulsive (positive). As a measure of the coupling strength, we consider the value of $\Delta\theta$ when $\theta = 0.5$, that is the phase shift, $\Delta\theta$, induced by coupling two drops whose initial phase difference is $\theta = 0.5$, or 180°. This particular choice for $\theta$ is somewhat arbitrary. Using this definition, we find that the repulsive coupling strength increases as the drop

 

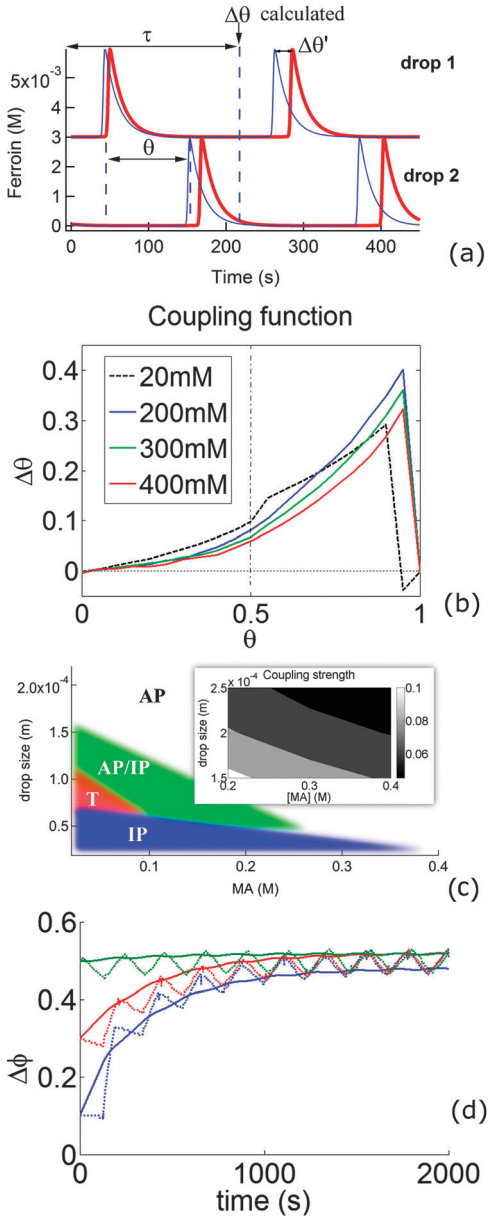


Fig. 4 Calculated coupling strength. (a) Ferroin concentration *vs.* time calculated using the FKN point-oscillator model for two drops such as illustrated in Fig. 2a in the out-of-phase condition. Thin blue lines: decoupled drops. Thick red lines: coupled drops. Drops are coupled at $t = 0$ and the phase shift ($\Delta\theta$) between the coupled and decoupled drops is calculated after one period ($\tau$) of the uncoupled system as a function of the initial phase shift ($\theta$) between the decoupled drops. Phase is normalized to 1. (b) Phase shift after one period of coupling ($\Delta\theta$) *vs.* initial phase shift ($\theta$) for different values of [MA] using the point oscillator model, with $P_{HBrO_2}$ = 0.1, $P_{Br_2}$ = 2.5, $P_{BrO_2}$ = 1, $a = b$ = 150 m. $\Delta\theta$ increases with $\theta$ and increases as [MA] decreases. (c) Phase diagram of attractor behavior as function of drop size and [MA] with the same partition coefficients as in Fig. 4b. The inset contour plot shows how the magnitude of $\Delta\theta$ for $\theta = \pi$ varies as a function of [MA] and drop size. IP: in-phase synchronization. AP/IP: bistability. T: stationary Turing state, in which some drops stop oscillating. (d) Dynamics of the phase difference between two oscillators ($\Delta\phi$) calculated with the point oscillator (dotted curves) and phase (solid curves) models using [MA] = 600 mM and the same geometry and partition coefficients as in Fig. 4b. $\Delta\phi_{t=0}$ = 0.1, 0.3, 0.5 for the blue, red, and green curves, respectively. Phase varies between 0 and 1.

size decreases, as the drop separation decreases, and as the malonic acid concentration decreases, consistent with our previous measure of coupling strength, $S$. We find that the coupling is purely repulsive for a wide range of conditions: 200 mM < [MA] < 2 M and drop size >100 μm, consistent with our previous observations with such drops.[1] For smaller drops or low [MA], bistable attractors, in-phase attractors and stationary Turing states appear. In Fig. 4b, for the case [MA] = 20 mM, the coupling function crosses zero, rendering it bistable, with an in-phase attractor above $\theta > 0.9$ and anti-phase otherwise. The dynamical phase behavior is summarized in Fig. 4c.

**(d) Validity of phase model.** We also studied the dynamics of phase coupling for a pair of droplets using the point oscillator model (Fig. 4d). Similar to eqn (10.13) to (10.17) in Izhikevich[27] and Section 5.2.2 in Kuramoto,[13] we define $\theta_i(t) = t/\tau + \phi_i(t)$, $i = 1, 2$ for phases of the two droplets, with the first term the phase of free-running oscillation ($\tau$ is the free-running period) and the second term the slow phase deviation induced by coupling these two droplets. In Fig. 4d we plot $\Delta\phi(t) = \phi_1(t) - \phi_2(t)$ as calculated from the point oscillator model and the phase model (eqn (1a) and (b)) for various initial conditions, $\Delta\phi_{t=0}$ = 0.1, 0.3, 0.5. For both models the phase difference evolves from the initial condition to a steady phase deviation, $\Delta\phi_{t\to\infty} = 0.5$, corresponding to anti-phase coupling. The results for the point oscillator model give the instantaneous phase difference (dotted lines), while the phase oscillator model (solid lines) represents only the slow dynamics, as the coupling function $H$ was obtained by averaging the coupling between drops over one period. The fact that $\Delta\phi$ corresponds for the point and phase models establishes the validity of the phase model for BZ droplets in the weak coupling limit.

### 3.4 Excitatory coupling and in-phase behaviors

**(a) Trigger wave.** Using [MA] = 40 mM and droplets in contact, or using [MA] = 20 mM and more closely spaced droplets than in Fig. 1, we were able to obtain a stable in-phase behavior of large arrays of 1D droplets as observed in Fig. 5(a–d). We were unable to observe such patterns for 40 mM < [MA] < 2 M. In contrast with previously reported unstable in-phase patterns,[3] the stable patterns found here often (but not always) initially begin with zero phase shift between adjacent drops and subsequently develop a small, but constant phase shift between adjacent droplets, creating a propagating BZ wave, analogous to the behavior observed in a continuous aqueous BZ solution.

We simulated the observed wave pattern using COMSOL to model a chain of 2D disks in oil. We postulated that the waves observed experimentally in Fig. 5b and d were trigger waves. To numerically explore this possibility we set one drop on the edge of the simulation box to have a higher concentration of sulfuric acid than the other drops, causing that drop to oscillate faster than the other drops and thus act as a trigger (Fig. 5g and h). We compared experiments showing traveling waves in drops in cylindrical capillaries with simulation and found similar behavior. To validate the simulations, we modeled a continuous BZ solution confined in the same capillary and compared with experiment. Again the simulation and experiment were similar,

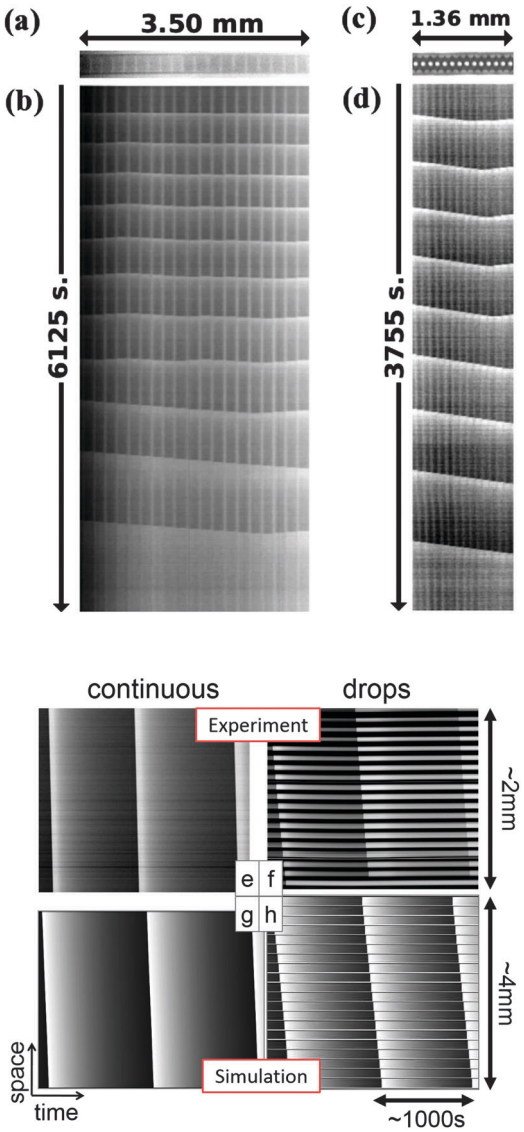


Fig. 5 In-phase patterns: trigger wave experiments *vs.* simulations. (a, c) photographs of drops in capillary. (b, d) Space-time plots. (a, b) [MA] = 20 mM, (c, d) [MA] = 40 mM. Droplet diameter is (a, b) 150 μm and (c, d) 97 μm; distance between droplets is (a, b) 36 μm and (c, d) touching droplets. (e) Experiment: single phase BZ solution ([MA] = 20 mM). Trigger wave speed 2 mm $min^{-1}$. (f) Experiment: BZ droplets (100 μm), trigger wave speed 1 mm $min^{-1}$. (g) Simulated in COMSOL, single phase using [MA] = 20 mM. Trigger wave speed, 4 mm $min^{-1}$. (h) Simulated in COMSOL, BZ droplets (200 μm), trigger wave speed 2 mm $min^{-1}$. The topmost droplet has slightly higher $[H^+]$ = 0.2 M than the rest of the droplets (0.16 M) to act as an intrinsically faster "trigger". $P_{HBrO_2}$ = 0, $P_{Br_2}$ = 2.5, $P_{BrO_2}$ = 5. Identical results are obtained with $P_{Br_2}$ = 2.5, $P_{HBrO_2} \approx 0.01$ and $P_{BrO_2}$ = 1.

as illustrated in Fig. 5(e–h). The one discrepancy was that the frequency of the oscillation in the simulation was about twice that found in the experiment. This is a shortcoming of the FKN model, and not a consequence of the finite element aspect of the calculation. This discrepancy in oscillation frequency led to the wave speed in simulation being twice as fast as in experiment; however, the calculated wavelength agreed with experiment. In both simulation and experiment, the speed of the trigger wave in the continuous BZ fluid was twice the speed of the wave in the chain of drops. The oil gap diminishes the diffusive flux in comparison to the continuous BZ solution, offering a possible explanation for the slower propagation speed in the drops.

To explore the origin of the temporal evolution of the phase between adjacent drops from initially zero phase to a constant phase as shown in Fig. 5, we repeated the trigger-wave simulations of Fig. 5g and h as a function of inter-drop coupling strength. In Fig. 6a we simulate a line of identical drops, except for one drop on the end, which has a higher frequency. The drop spacing is 60 microns, large enough that the fast drop does not launch a trigger wave, but the drops are still sufficiently coupled to oscillate in phase. Simulated light was shone on the middle drop with sufficient intensity to suppress oscillation in that drop. One observes that drops immediately adjacent are slightly influenced by the increased bromine produced by the illuminated drop.

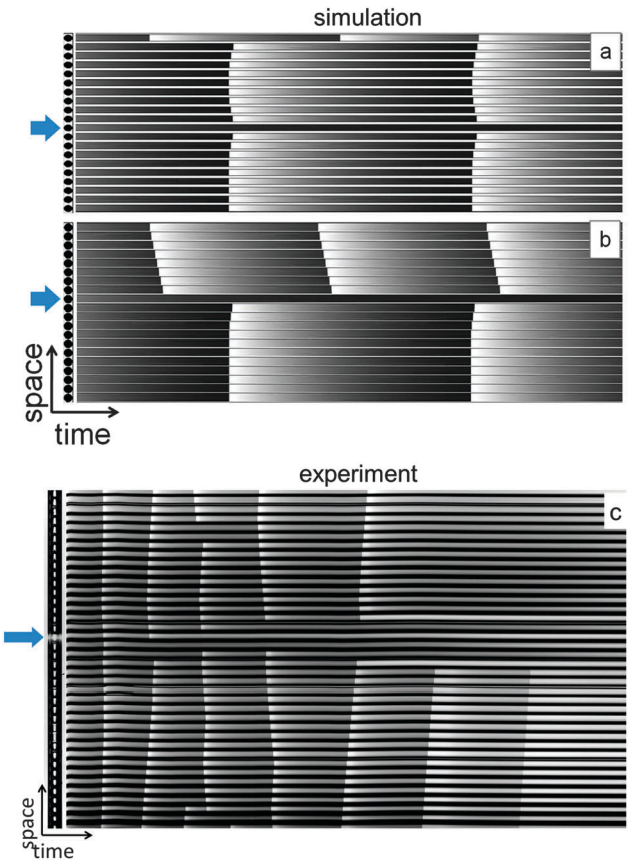


Fig. 6 Traveling waves and coupling strength. Blue arrows indicate light-suppressed BZ drops. (a, b) COMSOL simulations ([MA] = 20 mM, $P_{HBrO_2}$ = 0, $P_{Br_2}$ = 2.5, $P_{BrO_2}$ = 5): (a) drop size *a* = 160 μm, oil gap *b* = 60 μm. (b) *a* = 200 μm, *b* = 20 μm, light intensity 0.01 $s^{-1}$ (pseudo concentration in the model). In both (a) and (b) the first drop (top, $[H^+]$ = 0.22 M) is made to oscillate faster than the other drops ($[H^+]$ = 0.16 M). The light-suppressed drop in the middle separates the drop array into two parts in each case. Trigger wave behavior is observed only in (b), where the inter-drop coupling is stronger, but in-phase attractors are observed for both (a) and (b). (c) Experiment ([MA] = 20 mM, *a* = 100 μm, *b* = 10 μm). Although the *a*/*b* ratio in this experiment is the same as in Fig. 6b, the result resembles Fig. 6a. The experiment started with an in-phase attractor with zero phase shift between drops and evolved into a trigger wave.

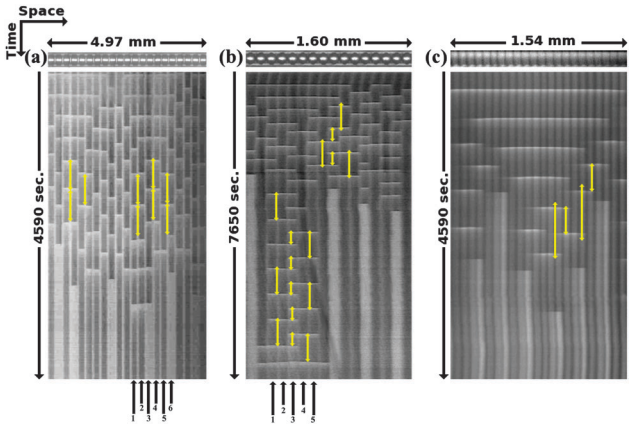


Fig. 7 Space-time plots of mixed mode patterns. (a) Droplets are 170 mm in diameter separated by 70 μm, [MA] = 20 mM. (b) Droplets of 100 μm diameter are in contact, [MA] = 40 mM. (c) Droplets of 70 μm diameter are in contact, [MA] = 60 mM. Before starting each experiment, the droplets were synchronized in-phase by illuminating the capillary with intense 450 nm light for about 10 min. In the space-time plots, long double arrows mark periods of at least two in-phase neighbor droplets; short arrows, half the size of the long arrows, mark the period of a single droplet.

In Fig. 6b the inter-drop separation is reduced to 20 μm. Now a trigger wave is formed, but does not propagate across the light-induced gap. From these simulations we conclude that trigger waves require a stronger coupling between drops than do in-phase attractors with zero phase shift between neighbors. Fig. 6c shows an equivalent experiment. The drop in the center of the capillary is illuminated, suppressing its oscillation. The drops initially oscillate with zero phase shift between neighbors, but with time, a traveling wave emerges as the malonic acid concentration decreases and the coupling strength consequently increases.

**(b) Cluster patterns.** In Fig. 7a, we present a space-time plot highlighting three pairs of in-phase droplets numbered 1–6. The pattern consists of a row of drops in which at a particular instant in time all drops form pairs where drops in a pair have the same phase, but each pair is 180° out-of-phase with its neighboring pairs, *i.e.* drops #1 and #2 have 0° phase, drops #3 and #4 have 180° phase and drops #5 and #6 have 0° phase. We refer to this pattern as a "local in-phase, global out-of-phase" attractor. In Fig. 7b we observe defects in this synchronization pattern that occur when there is an additional drop separating two pairs, *i.e.* drops #1 and #2 have 0° phase, drops #4 and #5 have 180° phase and drop #3 is the defect. In this case, the droplet separating the two pairs (drop #3) alternately synchronizes in-phase with the neighboring pairs to each side; a feat that is only possible when the middle droplet oscillates with twice the frequency of its neighbors. As in the case of the stable in-phase patterns in Fig. 5, the patterns observed in Fig. 7 require low [MA] and/or droplets with small separation. We observed these local in-phase – global out-of-phase modes for [MA] up to 60 mM, as observed in Fig. 7c. At higher [MA], even touching droplets yield only out-of-phase patterns.[1] Typically, as the BZ reaction proceeds towards equilibrium, oscillations eventually give way to a stationary Turing pattern with some drops locked in the oxidized state and others in the reduced state.

Often, the local in-phase – global out-of-phase pattern is mixed with "pure" out-of-phase behavior or with stationary droplets. In Fig. 7a, on either side of the pairs of highlighted arrowed regions, we observe drops where nearest neighbors are out-of-phase, while in Fig. 7b the right side of the space-time plot shows stationary droplets while the left side remains oscillatory. When the pattern includes stationary droplets, as observed in Fig. 7b and c, the stationary droplets produce a variety of complex, often symmetric, patterns. In Fig. 7c we observe periodic stationary Turing patterns with wavelengths of 4 drops; in Fig. 7b the Turing wavelength is 3 drops. The most commonly observed in-phase clusters consist of a pair of droplets, and the number of droplet clusters drops off sharply with the size of the cluster.

All our models (Vanag and Epstein,[2] Fig. 4) predict that if drops are in a stationary Turing state and the coupling is increased, then the drops should resume oscillating, but in-phase. We have not observed this behavior for drops in 1D capillaries. At this time, it is not clear if this is because the theory is wrong, that we have not found the right experimental conditions, or, most probably, the assumption that the closed system as a function of time corresponds to an open system with decreasing malonic acid concentration fails.

**(c) Transport of BZ species through the oil.** The occurrence of stable in-phase patterns suggests excitatory coupling between droplets. The permeability and chemical reactivity of the BZ products in the perfluorinated oil that we use have not been fully characterized. This oil is slightly polar, with a dielectric constant of 5.8, whereas octane, which was employed in earlier studies of BZ emulsions,[5] has a dielectric constant of 1.9.[28] As we show below, this perfluorinated oil acts as a transport medium for slightly polar molecules such as oxyhalogens and weak acids. To investigate the transport of weak acids, we placed two water droplets separated by a fluorinated oil gap inside a hydrophobized capillary. One droplet contained a ~1 M solution of a weak acid, while the other had a 6 mM solution of the pH indicator thymol blue at pH 8.[29] We studied chloroacetic, iodoacetic, and malonic acids. Equal volumes of the thymol blue solution and any of these acids gave an intense red-pink solution. Fig. 8 shows a typical example of these experiments with malonic acid. The drop containing thymol blue (on the left) becomes darker as time goes on, indicating the transport of MA through the fluorinated oil. Moreover, the oil also becomes darker in time. This demonstrates that a small amount of the indicator partitions into the oil phase, which can be explained by the fact that thymol blue is an uncharged weak acid in its completely protonated red form. Similar results were obtained for chloroacetic and iodoacetic acids. From these observations, we conclude that mass exchange of uncharged weak acids, like MA and $HBrO_2$, takes place between droplets in this fluorinated oil. In contrast to the weak acids, similar experiments with sulfuric acid, a strong acid, gave no evidence of permeation through the oil.

To estimate the interdrop transport of bromine dioxide radical ($BrO_2^{\bullet}$), which is too reactive to employ in these experiments, we used the chemically similar, but stable molecule, chlorine dioxide, $ClO_2^{\bullet}$. As described in the Methods section, $ClO_2^{\bullet}$ was generated in drops by mixing sodium chlorite with

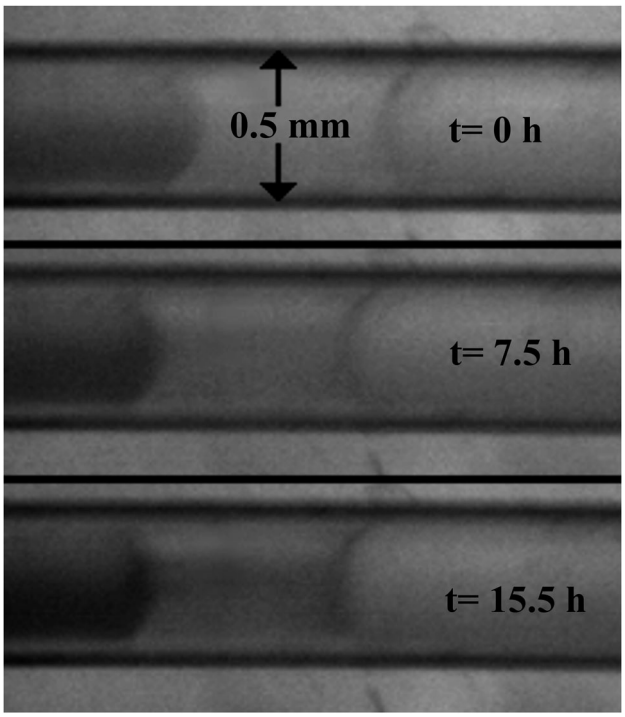


Fig. 8 Activator permeation. From top to bottom, three pictures of the same capillary (0.5 mm internal diameter) with increasing time. At the left, a droplet of thymol blue, which darkens with time; at the right, a reservoir of 1.3 M malonic acid. Fluorinated oil HFE-7500 in the center also becomes darker in time, revealing the presence of the nonionic form of thymol blue in the oil. The capillary is observed with 510 nm light.

nitric acid. It took about 20 minutes for the [$ClO_2^\bullet$] concentration to reach a maximum inside a drop and about 50 minutes for the [$ClO_2^\bullet$] in the oil to exceed that in the drop. In contrast, the transport of the inhibitor, $Br_2$, from drop to oil is immeasurably rapid. In the 30 seconds that it takes to load the capillary with droplets, remove it from the microfluidic chip and place it in the microscope for observation, a significant fraction of the bromine has left the drop and come to equilibrium with the oil drop. These results suggest that the rate of $BrO_2^\bullet$ transport between droplets is two or more orders of magnitude slower than $Br_2$ transport through the same interface.

The results described in the two previous paragraphs demonstrate that the transport of $Br_2$ from the water through the fluorinated oil is much faster than the transport of all the other species tested here, *i.e.*, $BrO_2^\bullet$, MA and the other weak acids. The permeation coefficient, defined as the product *PD*,[30] governs the flux of chemicals between drops, where *P* is the partition coefficient and *D* is the diffusion coefficient. *D* varies only slightly between molecular species and cannot account for the large difference between transport rates of the different species. However, *P* can vary by orders of magnitude among the BZ chemical species. For $Br_2$ we have previously measured *P* in this oil as 2.5,[1] while for $ClO_2^\bullet$ we measured the partition coefficient between oil and water spectrophotometrically after extraction in the bulk, yielding $P = 1.2$. The value of the permeability for $Br_2$ is at least twice the value of any of the other tested chemical species.

The experiments described in this section strongly support our hypothesis that excitatory coupling caused by the transport of $BrO_2^\bullet$ and $HBrO_2$ through the oil plays a major role in facilitating the observed in-phase behavior at low [MA]. In the next section we describe experiments based on this hypothesis that are designed to enhance excitatory coupling.

**(d) Excitatory coupling enhancement: observation and consequences.** Two ways were explored to enhance excitatory coupling. First, decreasing the concentration of $Br_2$ should weaken the inhibitory coupling, thereby making the excitatory coupling more effective. Second, increasing the concentration of $HBrO_2$ and/or $BrO_2^\bullet$ should directly strengthen the excitatory coupling between droplets.

Exploring the first approach, we confirmed that MA and $Br_2$ are able to react in the fluorinated oil, probably to give dibromomalonic acid *via* a classic addition of bromine to a double bond in a nonaqueous solvent.[31] This reaction removes $Br_2$ directly and thereby diminishes the production of bromide, the major BZ inhibitory species, in the water drop. In an earlier study,[1] we reported out-of-phase patterns at [MA] = 2.8 M and moderately spaced droplets. By increasing [MA] to 2.9 M and placing the droplets in contact, we were able to generate in-phase trigger wave oscillatory behavior that was maintained for about a dozen cycles, as shown in Fig. 9. Neither our point oscillator nor our finite element model predicts in-phase oscillations at [MA] $>$ 2.8 M. Our numerical models do not account for any chemical reactions in the oil phase. However, we expect that eliminating the inhibitory species, but not the excitatory species from the oil phase will lead to in-phase oscillation. As a function of time, the [MA] concentration decreases, and below a threshold of 2.8 M the in-phase oscillations will transform to out-of-phase behavior. As in Fig. 1, in-phase droplets oscillate with a shorter period than when they oscillate out-of-phase. Another interesting observation is that the speeds of the trigger waves associated with the in-phase patterns at [MA] = 40 mM (Fig. 5) and 2.9 M (Fig. 9), are the same.

Next, we examine the effect of direct enhancement of the excitatory coupling by increasing the activator concentration in the oil, *via* the aqueous reaction $HBrO_2 + BrO_3^- + H^+ \leftrightarrow 2BrO_2 + H_2O$, which is a key step in the FKN mechanism.[10] We expect that $BrO_2^\bullet$ is more soluble in oil than the more polar $HBrO_2$ (although it, too, may permeate into the oil); therefore increasing the bromate and acid concentrations should shift the

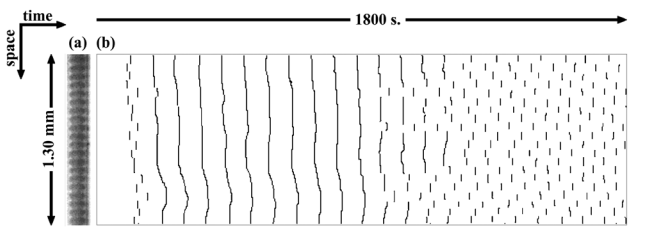


Fig. 9 High malonic acid. (a) Droplets of 65 μm diameter are in contact, [MA] = 2.9 M. (b) Space-time plot showing a transient in-phase trigger wave pattern followed by an out-of-phase pattern. The moments when the oxidized state flash occurs are enhanced for clarity.

 

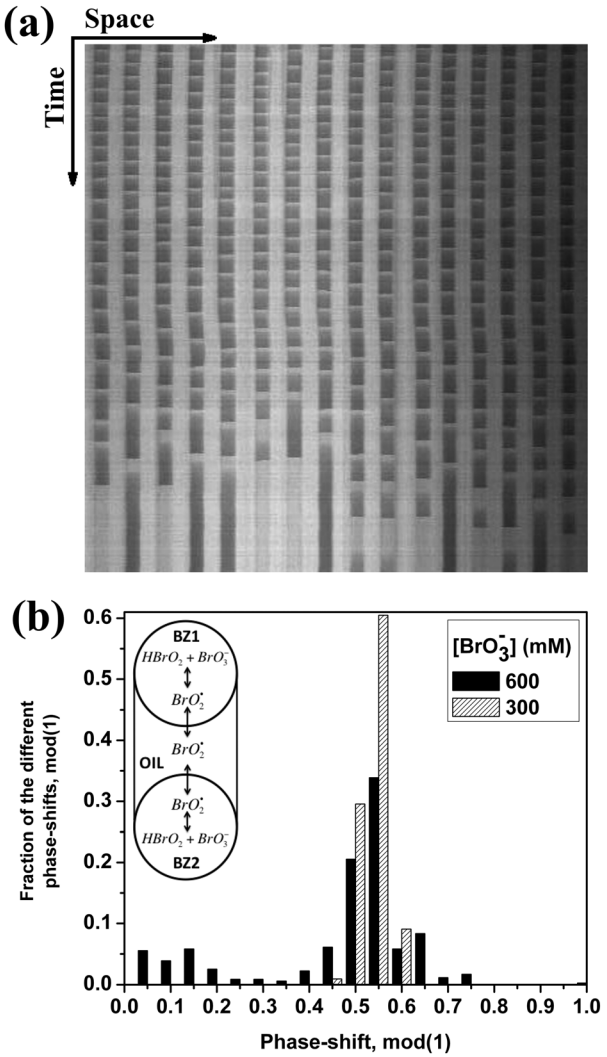


Fig. 10 Activator coupling. (a) Space-time plot for [MA] = 60 mM, [$BrO_3^-$] = 600 mM and [$H_2SO_4$] = 160 mM. Droplets are 170 μm in diameter and 190 μm apart. The total time of the space-time plot is 2000 s. (b) Distribution of phase-shifts of pairs of neighboring droplets under the conditions of (a) (black bars), compared with the distribution when [MA] = 60 mM, [$BrO_3^-$] = 300 mM and [$H_2SO_4$] = 80 mM (shaded bars). Inset suggests a possible mechanism of excitatory coupling.

equilibrium to the right, increasing [$BrO_2^\bullet$] and thereby strengthening the excitatory coupling through the oil.

Our earlier work[1] found that with concentrations of [$H_2SO_4$] = 80 mM and [$BrO_3^-$] = 300 mM, a 60 mM malonic acid concentration produced robust anti-phase patterns. Fig. 10a shows a space-time plot at [MA] = 60 mM and twice the previous concentrations of bromate and sulfuric acid. We ran this experiment without initially synchronizing the droplets in-phase. Fig. 10 compares the distribution of phase shifts between neighboring droplets under stationary conditions[1] with the two sets of acid and bromate concentrations. We argue that the relative strength of excitatory to inhibitory coupling correlates with the phase difference between coupled oscillating drops; inhibitory-dominated coupling leads to phase repulsion, in which neighbors have phase differences of half a cycle, whereas excitatory-dominated coupling results in phase attraction, where nearest neighbors have the same phase. The existence of in-phase pairs is clear at the higher bromate and acidity conditions; therefore increasing bromate increases excitatory coupling.

## 4. Conclusions

While we have not been able to manipulate the inhibitory and excitatory coupling completely independently, the present experimental system affords considerably more control over coupling than experiments in which interaction between oscillators occurs *via* an aqueous phase, so that all species participate in proportion to their concentrations,[4] or systems in which the inhibitor dominates the coupling between droplets.[1,3,5] Numerical investigations of the complex patterns that we observe suggest that both excitatory and inhibitory coupling are involved.

The fact that our experimental system is closed prevents us from obtaining true attractors, but the persistence of patterns that exhibit the same qualitative behavior for many cycles of oscillation suggests that these behaviors would be stable if we were able to maintain constant conditions indefinitely. This conjecture is supported by the striking similarities of even the most complex patterns in our experiments with the results of the simulations in open systems (for example, compare our Fig. 7b with Fig. 12e of ref. 2), which represent true attractors.

The main conclusions are

(1) The dynamical phase behavior of a chain of BZ drops is a function of coupling strength. As coupling strength increases, the following sequence is observed in experiment and numerical models (Fig. 4c): anti-phase, bistable anti-phase and in-phase/stationary Turing states, in-phase.

(2) Malonic acid concentration controls the coupling between BZ drops in oil by varying the balance between excitatory and inhibitory coupling. Mechanistically, malonic acid removes the inhibitor; therefore decreasing malonic acid increases inhibitory coupling. Drop size is a more dominant factor in coupling strength than the length of the oil gap. Theory suggests inhibitory coupling strength is characterized by $S = (PD)/(a(a + b)k_{eff})$.

(3) Numerical models demonstrate that weak coupling solely through the inhibitors, $Br_2$ and $Br^-$, produces phase repulsive coupling, leading to anti-phase synchrony, while coupling solely with activators, $HBrO_2$ or $BrO_2^\bullet$, produces attractive phase coupling, leading to in-phase synchrony. Strong inhibitory coupling also produces in-phase synchrony; essentially the drops lose their individual identities and effectively act as a single drop in the strong coupling limit. The transition from weak to strong coupling is marked by a transition from out-of-phase to in-phase synchrony and occurs at $S \sim 1$.

(4) Comparing a finite element model to experiment, we conclude that $Br_2$, $BrO_2^\bullet$, and $HBrO_2$ exchange between drops with partition coefficients $P_{Br_2} \backsimeq 2.5$, $P_{BrO_2} \backsimeq 1$, and $P_{HBrO_2} \backsimeq 0.01$; both excitatory and inhibitory coupling need to be included in the models to agree with the experiments.

(5) The point oscillator model qualitatively agrees with experiment and a realistic 3D finite element model.

(6) An accurate phase model was constructed for the case of weak coupling and anti-phase attractors.

(7) Malonic acid concentration decreases with time in the closed system of microfluidic drops. In contrast, our numerical models consider the malonic acid concentration to be constant.

(8) Malonic acid and bromine react in the oil, which is not accounted for in our numerical models.

(9) Simple numerical models account for the majority of the observations.

## Acknowledgements

N. Li, J. Delgado and H. González-Ochoa acknowledge support from the National Science Foundation Brandeis MRSEC-0820492 and use of the MRSEC microfluidics facility. We also acknowledge support from NSF grant CHE-1012428 and Army Research Office grant W911 NF-09-1-0496. We thank Vladimir Vanag for discussions and for suggesting measuring the transport of activators through the oil.

## References

1 J. Delgado, N. Li, M. Leda, H. O. González-Ochoa, S. Fraden and I. R. Epstein, *Soft Matter*, 2011, **7**, 3155.
2 V. K. Vanag and I. R. Epstein, *Phys. Rev. E: Stat., Nonlinear, Soft Matter Phys.*, 2011, 84.
3 M. Toiya, H. O. González-Ochoa, V. K. Vanag, S. Fraden and I. R. Epstein, *J. Phys. Chem. Lett.*, 2010, **1**, 1241.
4 A. F. Taylor, M. R. Tinsley, F. Wang, Z. Y. Huang and K. Showalter, *Science*, 2009, **323**, 614.
5 M. Toiya, V. K. Vanag and I. R. Epstein, *Angew. Chem., Int. Ed.*, 2008, **47**, 7753.
6 B. T. Ginn, B. Steinbock, M. Kahveci and O. Steinbock, *J. Phys. Chem. A*, 2004, **108**, 1325.
7 H. Fukuda, N. Tamari, H. Morimura and S. Kai, *J. Phys. Chem. A*, 2005, **109**, 11250.
8 N. Tompkins, N. Li, C. Girabawe, M. Heymann, G. B. Ermentrout, I. R. Epstein and S. Fraden, *Proc. Natl. Acad. Sci. U. S. A.*, 2014, **111**, 4397–4402.
9 R. J. Field and R. M. Noyes, *J. Chem. Phys.*, 1974, **60**, 1877.
10 R. J. Field, R. M. Noyes and E. Körös, *J. Am. Chem. Soc.*, 1972, **94**, 8649.
11 COMSOL In http://www.comsol.com/showroom/gallery/258/.
12 A. M. Turing, *Philos. Trans. R. Soc., B*, 1952, **237**, 37.
13 Y. Kuramoto, *Chemical oscillations, waves, and turbulence*, 2003.
14 Y. N. Xia and G. M. Whitesides, *Angew. Chem., Int. Ed.*, 1998, **37**, 551.
15 D. Qin, Y. N. Xia and G. M. Whitesides, *Nat. Protoc.*, 2010, **5**, 491.
16 C. Holtze, A. C. Rowat, J. J. Agresti, J. B. Hutchison, F. E. Angile, C. H. J. Schmitz, S. Koster, H. Duan, K. J. Humphry, R. A. Scanga, J. S. Johnson, D. Pisignano and D. A. Weitz, *Lab Chip*, 2008, **8**, 1632.
17 T. Lehtimaa, V. Tarvo, G. Mortha, S. Kuitunen and T. Vuorinen, *Ind. Eng. Chem. Res.*, 2008, **47**, 5284.
18 A. K. Horváth, I. Nagypál, G. Peintler, I. R. Epstein and K. Kustin, *J. Phys. Chem. A*, 2003, **107**, 6966.
19 A. M. Zhabotinsky, F. Buchholtz, A. B. Kiyatkin and I. R. Epstein, *J. Phys. Chem.*, 1993, **97**, 7578.
20 F. W. Schneider, *Annu. Rev. Phys. Chem.*, 1985, **36**, 347.
21 M. Dolnik, I. Schreiber and M. Marek, *Physica D*, 1986, **21**, 78.
22 V. Mendez, S. Fedotov and W. Horsthemke, *Reaction-Transport Systems: Mesoscopic Foundations, Fronts, and Spatial Instabilities*, Springer, Berlin, 2010.
23 A. T. Winfree, *The geometry of biological time*, Springer, 2001, vol. 12.
24 Y. Kuramoto, *Chemical oscillations, waves, and turbulence*, eqn. 5.2.17b, 2003.
25 E.M. Izhikevich, *Dynamical Systems in Neuroscience*, eqn 10.16, 2007.
26 J. Miyazaki and S. Kinoshita, *Phys. Rev. Lett.*, 2006, 96.
27 E. M. Izhikevich, *Dynamical Systems in Neuroscience*, 2007.
28 W. M. E. Haynes, *CRC Handbook of Chemistry and Physics*, CRC Press, NY, 91st edn, 2010.
29 E. E. Bishop, *Indicators*, Pergamon Press, Germany, 1972.
30 E. L. Cussler, *Diffusion mass transfer in fluid systems*, Cambridge University Press, USA, 2nd edn, 1997.
31 R. Morrison, *Organic chemistry*, 1992.

 